Ambiguity-resolved positioning performance in interferometric systems
Can constraining phase biases play a decisive role?

Khodabandeh, Amir; Yang, Songfeng; Teunissen, Peter J.G.

DOI
10.33012/2025.19988

Publication date
2025

Document Version
Final published version

Published in
Proceedings of the 2025 International Technical Meeting, ION ITM 2025

Ambiguity-resolved positioning performance in interferometric systems: Can constraining phase biases play a decisive role?

Amir Khodabandeh, *Faculty of Engineering and Information Technology, The University of Melbourne, Australia*
Songfeng Yang, *Faculty of Engineering and Information Technology, The University of Melbourne, Australia*
Peter J.G. Teunissen, *Department of Geoscience and Remote Sensing, Delft University of Technology, Delft, The Netherlands*

BIOGRAPHY

Amir Khodabandeh is a Senior Lecturer in Geodesy and Satellite Positioning at the Department of Infrastructure Engineering, the University of Melbourne, Australia. His research interests include geodetic estimation theory, interferometric positioning, and GNSS quality control.

Songfeng Yang is a Ph.D. student in Geomatics at the Department of Infrastructure Engineering, the University of Melbourne, Australia. His research interests lie in the field of Low-Earth-Orbit (LEO) signal-augmented PPP-RTK. He completed his BSc degree in Geodesy and Geomatics Engineering at Wuhan University, China, in 2019, and subsequently received his MSc degree in Geodesy and Survey Engineering from the same university in 2022.

Peter J.G. Teunissen is a Professor of Geodesy and Satellite Navigation at Delft University of Technology, the Netherlands, and a member of the Royal Netherlands Academy of Arts and Sciences. He has been research-active in various fields of earth observation, with current research focusing on developing theory, models, and algorithms for high-accuracy applications of satellite navigation and remote sensing systems. He is a fellow of ION and a recipient of the ION Kepler Award.

ABSTRACT

To fully utilize carrier phase measurements in high-precision interferometric positioning systems, such as global navigation satellite systems (GNSS), the corresponding integer ambiguities must be successfully resolved. Since the phase ambiguities are biased by non-integer phase delays, only specific combinations are allowed to serve as valid inputs for Integer Ambiguity Resolution (IAR) methods. Consequently, the resultant ambiguity-resolved phase data may not improve position precision as significantly as when all the ambiguities are resolved. The goal of this contribution is to study the role of phase biases in IAR and quantify the effect of bounding such biases in the ambiguity-resolved positioning performance. By identifying the interrelationship of the model's solutions, we show how constraining the phase biases has the potential to improve the precision of both the position and the ambiguities. With the aid of simulated results, it is illustrated that one can leverage the boundedness property of phase biases to obtain positioning results that are considerably more accurate than those obtained when the bias constraint is discarded.

I. INTRODUCTION

High-precision interferometric positioning systems such as Global Navigation Satellite Systems (GNSS) (Hofmann-Wellenhof et al., 2008; Teunissen and Montenbruck, 2017), interferometric wireless networks (Maróti et al., 2005; Wang et al., 2015), and opportunistic navigation with nonconventional sensors (Shamaei and Kassas, 2019) rely on the provision of carrier phase measurements. To fully exploit these ultra-precise measurements, the corresponding offsets must be successfully resolved during the estimation process. The offsets consist of arbitrary cycle counts, called integer ambiguities, and fractional phase biases caused by each of the transmitter and receiver clocks. Due to the linear dependency between the integer ambiguities and the phase biases, only certain combinations of the ambiguities satisfy the *integer-estimability* conditions (Teunissen and Odijk, 2003; Teunissen, 2019), the conditions that dictate whether or not the solution of such combinations can serve as an admissible input to Integer Ambiguity Resolution (IAR) methods like LAMBDA (Teunissen, 1993; Teunissen et al., 1997). As a consequence, a subset of the ambiguities cannot be resolved as they are absorbed by the corresponding estimable phase biases. Depending on the strength of the underlying measurement model, solutions of the remaining integer-estimable ambiguities may then be successfully mapped to their correct integers, thus essentially constructing ambiguity-resolved carrier phase data to enable high-precision model parameter solutions. The decision whether or not such integer-mapping is deemed successful is determined by the probability of correct integer estimation, the so-called ambiguity success-rate (Teunissen, 1999). When the ambiguity success-rate is not sufficiently large, it is likely that the output of the IAR method does not represent the sought-for

 https://doi.org/10.33012/2025.19988

integer-estimable ambiguities, seriously deteriorating the precision of the remaining parameter solutions. In that case, one may resign oneself to the *float* solution of the integer-estimable ambiguities, i.e., a real-valued ambiguity solution for which the integer property of the ambiguities is discarded. With the float ambiguity solution on the other hand, the parameters of interest (e.g., GNSS-derived position coordinates) fail to experience significant precision improvement (Khodabandeh and Teunissen, 2018).

In this contribution we aim to investigate the role of non-integer phase biases in influencing the model's ambiguity success rate, thereby addressing whether or not constraining such biases can help improve the precision of the positioning parameter solutions. In the literature, estimable forms of the phase biases are either estimated along with the other model parameters or eliminated from the model through, e.g., forming double-differences of the carrier phase measurements (Hofmann-Wellenhof et al., 2008). It has not yet been addressed if the IAR performance can benefit from the information about the extreme values that such phase biases can take on. Therefore, we study the condition under which bounding the stated biases increases the ambiguity success-rate. In doing so, we employ the recently developed integer-search method of BEAT (Khodabandeh, 2022) so as to incorporate the phase-bias constraint into the IAR process. To have the results generally applicable to the measurement systems with *frequency-varying* carrier phase signals like GLONASS or Low-Earth-Orbiting (LEO) communication satellites, we make use of the integer-estimable formulation (Khodabandeh and Teunissen, 2023). By 'frequency-varying', we mean that the signal frequencies are assumed to vary from transmitter to transmitter, while they remain unchanged over time. The (linearized) rank-deficient observation equations of such frequency-varying signals take the following form

$$\mathsf{E}(y) = A\,\overbrace{(z + B\delta)}^{a} + C\,c, \qquad (y \in \mathbb{R}^m,\ z \in \mathbb{Z}^n,\ \delta \in \mathbb{R}^q,\ c \in \mathbb{R}^p) \tag{1}$$

where the symbol $\mathsf{E}(\cdot)$ denotes the expectation operator, and y is the random vector of observables with $[A, C]$ being the augmented design matrix of full-column rank. The system (1) is rank-defect because the phase-bias vector δ is not separable from the integer ambiguity vector z. The corresponding full-column rank matrix B links δ to the real-valued ambiguity vector $a = z + B\delta$. A prime example of (1) is given by the linearized model of GNSS observation equations, with y containing the carrier phase and pseudorange (code) observables and c containing *estimable* forms of the remaining unknown parameters, such as e.g., position coordinates, atmosphere parameters, receiver and satellite clock parameters, and code delays.

Let us now assume that the phase-bias design matrix can be expressed as $B = Z_2 H$ for some $H \in \mathbb{R}^{q\times q}$, in which the $n \times q$ matrix Z_2, together with the $n \times (n-q)$ matrix Z_1, forms an *admissible integer transformation* $Z = [Z_1, Z_2]$. Therefore, by definition, the entries of both Z and its inverse $Z^{-1} = [\tilde{Z}_1, \tilde{Z}_2]^T$ are integer-valued (Teunissen, 1995). The inverse matrix Z^{-1} would then decompose the original ambiguity vector $z \in \mathbb{Z}^n$ into two parts, 1) the integer-estimable part $\tilde{z}_1 = \tilde{Z}_1^T z$ and 2) the integer-inestimable part $\tilde{z}_2 = \tilde{Z}_2^T z$, that is, $z = Z_1\tilde{z}_1 + Z_2\tilde{z}_2$. This follows by pre-multiplying the ambiguity vector z by both sides of the matrix identity $I_n = [Z_1, Z_2][\tilde{Z}_1, \tilde{Z}_2]^T$. As a result, the full-rank, *integer-estimable parametrized* version of (1) can be given as (Khodabandeh and Teunissen, 2023)

$$\mathsf{E}(y) = A\,\overbrace{(Z_1\tilde{z}_1 + Z_2\,\tilde{b})}^{a} + C\,c, \qquad (\tilde{z}_1 \in \mathbb{Z}^{(n-q)},\ \tilde{b} \in \mathbb{R}^q) \tag{2}$$

where $\tilde{b} = b + \tilde{z}_2$, in which $b = H\delta$ represents the phase bias vector δ in the Z-transformed domain. The real-valued ambiguity vector $a = z + Z_2\,b$ can now be equivalently expressed as $a = Z_1\,\tilde{z}_1 + Z_2\,\tilde{b}$. The vector $\tilde{b}$ represents the estimable version of b. The integer-estimable ambiguity vector $\tilde{z}_1$ is separable from $\tilde{b}$, but at the expense of lumping the integer-inestimable part $\tilde{z}_2$ with b. Our goal is to compare the IAR performance of (2) with its *bias-bounded* version (Khodabandeh and Teunissen, 2024)

$$\mathsf{E}(y) = AZ_1\,\tilde{z}_1 + AZ_2\,\underbrace{(b + \tilde{z}_2)}_{\tilde{b}} + C\,c, \qquad (\tilde{z}_1 \in \mathbb{Z}^{(n-q)},\ \tilde{z}_2 \in \mathbb{Z}^q,\ ||b|| \le h) \tag{3}$$

In comparison to (2), the bias-bounded model (3) is augmented with an extra piece of information, namely, the constraint $||b|| \le h$ which states that the magnitude of the unknown phase bias vector b is not larger than a positive scalar h. Imposing this extra constraint is to enable one to resolve, next to $\tilde{z}_1$, also the integer-inestimable ambiguity vector $\tilde{z}_2$. As far as the precision of the position solution is concerned, resolving the extra ambiguity vector $\tilde{z}_2$ would only be beneficial if

- the float solution of $\tilde{z}_2$, say $\hat{\tilde{z}}_2$, is *correlated* with that of the positioning parameters, that is, mapping $\hat{\tilde{z}}_2$ to $\tilde{z}_2$ improves position precision; and/or
- the float solution $\hat{\tilde{z}}_2$ is *correlated* with that of the existing integer-estimable ambiguities $\tilde{z}_1$, that is, mapping $\hat{\tilde{z}}_2$ to $\tilde{z}_2$ improves the precision of $\hat{\tilde{z}}_1$, thereby helping realize successful resolution of $\tilde{z}_1$.

We identify a condition under which the above two propositions are valid. When bias is present, but bounded, we take recourse to simulation to study the positioning precision improvement brought by the constraint $||b|| \leq h$.

The remainder of this paper is organized as follows. In Section II, we take the system of GNSS short-baseline observation equations as leading example, briefly reviewing the corresponding full-rank integer-estimable parametrized model. Since the applicability of the model also holds for frequency-varying signals, the role of the GNSS receivers can be taken by a pair of software-defined radios tracking signals of Low Earth Orbit (LEO) communication satellites (Khalife and Kassas, 2023). Although the carrier-phase measurements of such satellites have not yet been publicly available so as to rigorously evaluate their statistical characteristics, here we assume that the Iridium LEO satellites have GNSS-like L-band precise measurements (Pratt et al., 1999; Kassas et al., 2019) and use simulated measurements to conduct an early feasibility study. Next to GPS and GLONASS examples, we therefore also give an example of the admissible transformation $Z = [Z_1, Z_2]$ and $Z^{-1} = [\tilde{Z}_1, \tilde{Z}_2]^T$ forming integer-estimable and -inestimable ambiguities of Iridium frequency-varying phase measurements. In Section III, we derive analytical expressions for the parameter solutions of the short-baseline model, addressing how constraining the unknown phase-bias b can improve the positioning performance. The biased-constrained Integer Least-Squares (ILS) estimation and its link to the well-known ILS estimation for resolving both the integer-estimable and -inestimable ambiguities $\tilde{z}_1$ and $\tilde{z}_2$ are reviewed. Section IV is devoted to numerical results. We study how the 'bias-constrained integer least-squares estimation' and its search method of BEAT leverage the bias constraint $||b|| \leq h$ of the observation equations (3), significantly improving the ambiguity success-rate for different values of the phase-bias bound h, and for *certain* frequencies of the carrier phase measurements. Provided that the phase-bias constraint is correctly specified, it is illustrated that more accurate ambiguity-resolved positioning solutions can be obtained. Finally, concluding remarks will be provided in Section V.

II. INTEGER-ESTIMABILITY IN SHORT-BASELINE MODELS

Suppose that a pair of GNSS receivers or software-defined radios collect carrier-phase and pseudorange (code) measurements from m transmitters. The corresponding observed-minus-computed, between-receiver single-differenced (SD) phase and code measurements are cast in the n-vectors ϕ and p, respectively. If the distance between the receivers is sufficiently short to neglect the presence of SD atmospheric delays experienced in the measurements, a full-rank model for the corresponding linearized observation equations can then be formed as (Khodabandeh and Teunissen, 2023)

$$\mathsf{E}(\underbrace{\begin{bmatrix}\phi\\ p\end{bmatrix}}_{y}) = \underbrace{\begin{bmatrix}\Lambda\\ 0\end{bmatrix}}_{A} a + \underbrace{\begin{bmatrix}G & e\\ G & e\end{bmatrix}}_{C}\underbrace{\begin{bmatrix}x\\ dt\end{bmatrix}}_{c} \tag{4}$$

where the diagonal matrix $\Lambda = \mathrm{diag}(\lambda_1, \ldots, \lambda_n)$ contains the transmitter-specific wavelengths λ_s ($s = 1, \ldots, n$). The $n \times 3$ matrix G contains the transmitter-to-receiver line-of-sight unit vectors, and the n-vector of ones is denoted by $e = [1, \ldots, 1]^T$. The full-rank model (4) is a special case of (2), i.e. $m = 2n$, in which the role of vector c is given by a 4×1 vector ($p = 4$) containing the 3×1 baseline position increment vector x and the *estimable* SD receiver clock offset dt. Here, the word 'estimable' is emphasized to indicate that the scalar dt does *not* represent the original SD receiver clock offset, but a version that is *biased* by the SD receiver code delays. This is why the SD receiver code delays are absent in (4). Here and in the following, potential code inter-channel biases are assumed to be absent or a-priori calibrated, see e.g., (Wanninger and Wallstab-Freitag, 2007; Sleewaegen et al., 2012; Aggrey and Bisnath, 2016; Henkel et al., 2016; Banville et al., 2018). The model is solvable for the unknown parameters x, dt and a, if the $n \times 4$ matrix $[G, e]$ is of full-column rank. The necessary condition is to have at least 4 transmitters, i.e. $n \geq 4$.

The full-rank model (4) can be directly used for positioning and navigation with 'frequency-varying' carrier phase observables. For the single-epoch case, i.e. when measurements of only one time-instance are considered, the phase data ϕ are fully reserved for the unknown estimable ambiguities $\tilde{a}$, meaning that it is only the code data p that contribute to the estimation of the position x. This is because the number of unknown ambiguities a is as many as that of the phase data ϕ. To involve ϕ in the estimation process, one should impose the integer constraint $z \in \mathbb{Z}^n$ on $a = z + B\,\delta$. For the special case of the baseline model (4), the full-rank matrix B reduces to the n-vector $B = \Lambda^{-1}e$, in which the scalar δ indicates the SD receiver phase delay expressed in units of length. Thus, $q = 1$. To have the representation $B = Z_2 H$ and identify the corresponding Z_2- and H-matrices, one needs to assume that the transmitter frequencies f_s, $s = 1, \ldots, n$, are *integer multiples* of a base frequency f_0, that is, $f_s = r_s\, f_0$ ($r_s \in \mathbb{Z}$). An illustrative example is the set of frequencies under which GLONASS FDMA operates, the ratios of which are currently given by

$$r_s = 2848 + \kappa_s,\ \kappa_s \in [-7, +6] \tag{5}$$

with $f_0 = 9/16$ MHz and $f_0 = 7/16$ MHz for the L1 and L2 bands, respectively. For the CDMA case in which all the frequencies are identical, i.e. $f_s = f_0$, these ratios are simply set to $r_s = 1$ ($s = 1, \ldots, n$). In the case of Iridium L-band

signals, the satellite frequencies are related to their base frequency f_0 as

$$f_s = r_s\, f_0, \quad (f_0 = 100\ \text{Hz}) \quad \text{with} \quad r_s \in \{16261042, 16261458, 16262708, 16263958, 16264375\} \tag{6}$$

With the aid of the relations $f_s = r_s\, f_0$ and $\lambda_s = c_o/f_s$ (with c_o being the speed of light in vacuum), substitution of $\lambda_s^{-1} = r_s\, \lambda_0^{-1}$ into $a = z + \Lambda^{-1} e\, \delta$ gives

$$a = z + \underbrace{Re}_{Z_2}\, \underbrace{(\frac{\delta}{\lambda_0})}_{b} \tag{7}$$

in which the base wavelength is given as $\lambda_0 = c_o/f_0$, with $R = \text{diag}(r_1, \ldots, r_n)$. Thus, $Z_2 = [r_1, \ldots, r_n]^T$ and $H = (1/\lambda_0)$. In (7), we assume that the greatest common divisor (GCD) of the ratios r_s is one. For the cases where the GCD is larger than one, the ratios can be down-scaled by being divided by their GCD. Under this assumption, the integer vector Re can act as the column Z_2 of the admissible transformation $Z = [Z_1, Z_2]$ (Teunissen, 2019). Given the input vector $Z_2 = Re$, the integer-sweeping algorithm returns the sought-for integer matrices Z_1 and $Z^{-1} = [\tilde{Z}_1, \tilde{Z}_2]^T$ as output. These outputs are used to form the integer-estimable parameterized version of (4). This version follows by substituting $a = Z_1 \tilde{z}_1 + \tilde{b}$ into (4), that is

$$\mathsf{E}(\underbrace{\begin{bmatrix} \phi \\ p \end{bmatrix}}_{y}) = \underbrace{\begin{bmatrix} \Lambda Z_1 \\ 0 \end{bmatrix}}_{AZ_1} \tilde{z}_1 + \underbrace{\begin{bmatrix} \Lambda Re \\ 0 \end{bmatrix}}_{AZ_2} \tilde{b} + \underbrace{\begin{bmatrix} G & e \\ G & e \end{bmatrix}}_{C} \underbrace{\begin{bmatrix} x \\ dt \end{bmatrix}}_{c} \tag{8}$$

With the above alternative full-rank model, one can involve the phase data ϕ in the estimation of the position increment x through resolving the integer-estimable ambiguities $\tilde{z}_1 = \tilde{Z}_1^T z$. In the next section, we present analytical expressions for the float solutions of model (8), addressing if information about the size of the transformed phase bias b in $\tilde{b} = b + \tilde{z}_2$ can enhance the precision of the solutions.

To conclude this section, we make a remark about the admissible transformation $Z = [Z_1, Z_2]$ and its inverse $Z^{-1} = [\tilde{Z}_1, \tilde{Z}_2]^T$. Depending on the values that the frequency ratios r_s ($s = 1, \ldots, n$) take on, the $n \times (n-1)$ matrix $\tilde{Z}_1$ dictates that the float solution of only *certain* integer combinations of the original ambiguities z is permitted to serve as an admissible input to IAR methods, while the integer vector $\tilde{Z}_2$ represents a combination of z which is to be absorbed by the estimable phase bias $\tilde{b}$. The $n \times (n-1)$ matrix Z_1 is used to structure the full-rank ambiguity design matrix AZ_1. To show numerical examples of such matrices, we employed the 'integer-sweeping' algorithm of (Teunissen and Khodabandeh, 2022, pp. 5) for three different satellite constellations of GPS, GLONASS and Iridium. The results are given in Table 1. For the GPS case, as one would expect, the algorithm returns the columns of $\tilde{Z}_1$ as *between-satellite differences*. This is because the GPS signals follow the CDMA strategy, having identical frequencies. For this case, the integer-estimable ambiguities $\tilde{z}_1 = \tilde{Z}_1^T z$ are the well-known double-differenced (DD) ambiguities. Likewise, the ambiguity of the first (pivot) satellite is chosen as the corresponding integer-inestimable ambiguity $\tilde{z}_2 = \tilde{Z}_2^T z$. Comparing the $\tilde{Z}_1$-matrix of GPS with those of GLONASS and Iridium, one recognizes that the integer-estimable ambiguities $\tilde{z}_1 = \tilde{Z}_1^T z$ of these two satellite systems are *not* formed by the traditional DD combinations as their corresponding Z_2-vector is *different* from the vector of ones e. The large entries of the bias design matrix AZ_2 indicate that the float solution of the estimable bias $\tilde{b}$ can become considerably more precise compared to the solutions of $\tilde{z}_1$. In the next section, we will make use of this very property and discuss its consequence when imposing the bias constraint $|b| \leq h$.

III. THE INTERRELATIONSHIP OF THE FLOAT SOLUTIONS

Although the full-rank model (8) enables one to perform IAR even for frequency-varying phase measurements, thereby forming the basis of FDMA ambiguity-fixing (Teunissen, 2019), several studies have reported that 'full' ambiguity resolution may not be always successfully carried out, restricting one to choose the option of *partial* ambiguity resolution, see e.g., (Teunissen and Khodabandeh, 2019; Brack et al., 2021; Zaminpardaz et al., 2021). To gain some insight into why such a restriction holds for existing frequency-varying phase measurements (e.g. those of GLONASS), let us compare the $\tilde{Z}_1$-matrix of the GPS case with its frequency-varying versions in Table 1. Due to the structure of the GLONASS and Iridium signal frequencies, their corresponding $\tilde{Z}_1$-matrix contains relatively large entries. As a consequence, the float ambiguity solution $\hat{\tilde{z}}_1$ contains poorly precise entries, hindering full IAR (Teunissen, 2019).

By switching to partial IAR on the other hand, the resultant ambiguity-resolved phase data do not improve position precision as impactful as their full IAR counterparts do. Considering the bias term $\tilde{b} = b + \tilde{z}_2$ in (8), one may be tempted to find a way to eliminate the unwanted bias parameter b in order to incorporate the float solution of the extra ambiguity $\tilde{z}_2$ into the IAR process, hoping to improve position precision. This is because, in the absence of b, the estimable bias $\tilde{b}$ reduces to the remaining

Table 1: Examples of the admissible integer transformation $Z = [Z_1, Z_2] \in \mathbb{Z}^{n\times n}$ and its inverse $Z^{-1} = [\tilde{Z}_1, \tilde{Z}_2]^T \in \mathbb{Z}^{n\times n}$ for three different satellite constellations of GPS, GLONASS and Iridium, in which the number of satellites is set to $n = 5$. With the integer vector $Z_2 = Re = [r_1, \ldots, r_n]^T$ as input, the 'integer-sweeping' algorithm delivers the remaining matrices Z_1, $\tilde{Z}_1$ and $\tilde{Z}_2$, see e.g., (Teunissen and Khodabandeh, 2022).

	$Z_2 = Re$	Z_1	$\tilde{Z}_1$	$\tilde{Z}_2$
GPS:	$\begin{bmatrix} 1 \\ 1 \\ 1 \\ 1 \\ 1 \end{bmatrix}$	$\begin{bmatrix} 0 & 0 & 0 & 0 \\ 1 & 0 & 0 & 0 \\ 0 & 1 & 0 & 0 \\ 0 & 0 & 1 & 0 \\ 0 & 0 & 0 & 1 \end{bmatrix}$	$\begin{bmatrix} -1 & -1 & -1 & -1 \\ +1 & 0 & 0 & 0 \\ 0 & +1 & 0 & 0 \\ 0 & 0 & +1 & 0 \\ 0 & 0 & 0 & +1 \end{bmatrix}$	$\begin{bmatrix} 1 \\ 0 \\ 0 \\ 0 \\ 0 \end{bmatrix}$
GLONASS:	$\begin{bmatrix} 2849 \\ 2841 \\ 2846 \\ 2852 \\ 2843 \end{bmatrix}$	$\begin{bmatrix} 1 & 1424 & 0 & 1 \\ 0 & 1420 & 0 & 1 \\ 0 & 1422 & 0 & 1 \\ 0 & 1425 & 1 & 1 \\ 0 & 1421 & 0 & 1 \end{bmatrix}$	$\begin{bmatrix} 1 & 0 & 0 & 0 \\ 3 & -3 & 3 & 1420 \\ 0 & -2 & -1 & -1 \\ 0 & 0 & 1 & 0 \\ -4 & 5 & -3 & -1418 \end{bmatrix}$	$\begin{bmatrix} 0 \\ +1 \\ +1 \\ 0 \\ -2 \end{bmatrix}$
Iridium:	$\begin{bmatrix} 16261042 \\ 16261458 \\ 16262708 \\ 16263958 \\ 16264375 \end{bmatrix}$	$\begin{bmatrix} 1 & 39089 & 0 & 8130521 \\ 1 & 39090 & 0 & 8130729 \\ 1 & 39093 & 0 & 8131354 \\ 1 & 39096 & 1 & 8131979 \\ 1 & 39097 & 0 & 8132187 \end{bmatrix}$	$\begin{bmatrix} 39063 & -625 & 0 & 1 \\ -39053 & 833 & 1 & -4 \\ -9 & -208 & -2 & 5 \\ 0 & 0 & 1 & 0 \\ 0 & 0 & 0 & -2 \end{bmatrix}$	$\begin{bmatrix} 1 \\ 0 \\ -2 \\ 0 \\ 1 \end{bmatrix}$

ambiguity $\tilde{z}_2$. Khodabandeh and Teunissen (2024) numerically illustrated that the bias term b, for the GLONASS FDMA case, is indeed small and bounded for several short baselines. An overview of the results is shown in Figure 1, in which the left and right panels represent the phase-bias estimates collected on 31st of March, and 30th of April 2023, respectively. As the figure indicates, while the estimates are bounded, their distribution may change over time. Instead of neglecting or calibrating such phase biases, one can impose the bounding constraint $|b| \leq h$ on the model. Would the boundedness property, shown in Figure 1, also carry over to other frequency-varying carrier-phase signals like those of the LEO satellites, quantifying the role of the constraint $|b| \leq h$ in their underlying IAR performance is then worthwhile.

1. Bias-bounded Integer Least-Squares

In quantifying the role of $|b| \leq h$, one may employ the bias-bounded Integer Least-Squares (ILS) estimation to solve the short-baseline model (8) for the involved parameters using the bias constraint $|b| \leq h$. The minimization problem underlying the general bias-bounded model (3) reads (Khodabandeh and Teunissen, 2024)

$$\min_{\tilde{z}_1\in\mathbb{Z}^{(n-q)},\tilde{z}_2\in\mathbb{Z}^q,c\in\mathbb{R}^p,||b||\leq h} ||\, y - AZ_1\tilde{z}_1 - AZ_2(\tilde{z}_2 + b) - C\, c\,||^2_{Q_{yy}} \tag{9}$$

with the short-hand notation $||\cdot||^2_{Q_{yy}} = (\cdot)^T Q_{yy}^{-1}(\cdot)$, and Q_{yy} being the variance matrix of the observation vector y. If the bias constraint $||b|| \leq h$ is lifted and replaced by $b \in \mathbb{R}^q$, problem (9) would not have a unique solution. This is because the unconstrained version of (3) is an under-determined system of equations where the number of unknowns is more than the number of equations. To have a unique minimizer for the above objective function, the non-negative scalar h is required to be smaller than certain values. For example, for the short-baseline model (8), h should not exceed half a cycle, that is, $h \leq 0.5$ (Khodabandeh, 2022).

As shown in Equations (12) and (13) of (Khodabandeh and Teunissen, 2024), for the case of (8), solving the minimization problem (9) leads to the following biased-bounded ILS solution for position x

$$\breve{x} = \hat{x} - Q_{\hat{x}\hat{\tilde{z}}_1} Q^{-1}_{\hat{\tilde{z}}_1\hat{\tilde{z}}_1} (\hat{\tilde{z}}_1 - \breve{\tilde{z}}_1) \tag{10}$$

Matrix $Q_{\hat{\tilde{z}}_1\hat{\tilde{z}}_1}$ denotes the variance matrix of the float ambiguity solution $\hat{\tilde{z}}_1$, while $Q_{\hat{x}\hat{\tilde{z}}_1}$ denotes the covariance matrix between the float solutions $\hat{x}$ and $\hat{\tilde{z}}_1$. Here, the notation $\breve{\cdot}$ is used to distinguish bias-bounded ILS solutions from their float versions indicated by $\hat{\cdot}$. The ambiguity solution $\breve{\tilde{z}}_1$ is searched as the integer minimizer of the following problem

$$\breve{\tilde{z}}_1 = \arg \min_{\tilde{z}_1\in\mathbb{Z}^{n-1}} \{||\hat{\tilde{z}}_1 - \tilde{z}_1||^2_{Q_{\hat{\tilde{z}}_1\hat{\tilde{z}}_1}} + P(\tilde{z}_1)\} \tag{11}$$

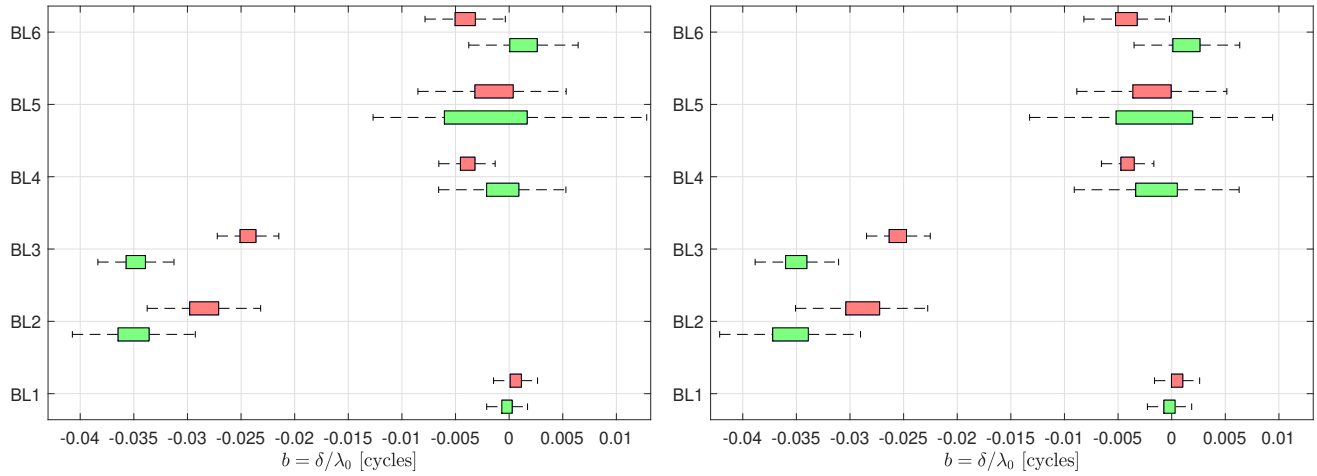

Figure 1: Boxplots of estimated values of the GLONASS FDMA phase bias $b = \delta/\lambda_0$ corresponding to 6 IGS zero/short-baselines: BL1 (ZIM2–ZIM3), BL2 (UNBD-UNBD3), BL3 (YARR-YAR2), BL4 (YARR-YAR3), BL5 (YEL2-YELL), and BL6 (YEL2-YEL3). The red and green boxes correspond to L1 and L2 frequency bands, respectively. The left and right panels represent the estimates collected on 31st of March, and 30th of April 2023, respectively, cf. (Khodabandeh and Teunissen, 2024).

in which the function $P(\tilde{z}_1)$ is specified as

$$P(\tilde{z}_1) = \frac{1}{\sigma_0^2} \min_{\tilde{z}_2 \in \mathbb{Z}, |b| \leq h} |\hat{\tilde{b}}(\tilde{z}_1) - \tilde{z}_2 - b|^2 \tag{12}$$

The scalar σ_0^2 denotes the variance of the *conditional* bias solution $\hat{\tilde{b}}(\tilde{z}_1)$. By 'conditional', we mean that the solution is conditioned on the assumption $\hat{\tilde{z}}_1 = \tilde{z}_1$ (see the next subsection for its expression). Note, for the unconstrained case $b \in \mathbb{R}$, that the function $P(\tilde{z}_1)$ vanishes as the bias can be simply set to $b = \hat{\tilde{b}}(\tilde{z}_1) - \tilde{z}_2$ for any $\tilde{z}_2 \in \mathbb{Z}$. For this case, i.e., when $P(\tilde{z}_1) = 0$, the integer minimizer (11) reduces to the well-known ILS solution of $\tilde{z}_1$ (Teunissen, 1999). For the constrained case $|b| \leq h$, the task of the function $P(\tilde{z}_1)$ is to downweight potential integer candidates $\tilde{z}_1 \in \mathbb{Z}^{n-1}$ if their corresponding conditional bias solution $\hat{\tilde{b}}(\tilde{z}_1)$ is further away from $\check{\tilde{z}}_2(\tilde{z}_1) + \check{b}(\tilde{z}_1)$, where $\check{\tilde{z}}_2(\tilde{z}_1)$ and $\check{b}(\tilde{z}_1)$ are the minimizers in (12). Thus, the bounded solution $\hat{\tilde{b}}(\check{\tilde{z}}_1)$ will have a better accuracy performance, since the function $P(\tilde{z}_1)$ penalizes out-of-bound solutions.

To carry out the integer search (11) and compute the bias-bounded ILS solution (10), one can employ the method of BEAT (Khodabandeh, 2022). To solve (11), BEAT utilizes the LAMBDA method (Teunissen, 1993) and sequentially searches for the minimizer $\check{\tilde{z}}_1$ inside a dual-ellipsoid encompassing region. For a detailed description of the search strategy, the reader is referred to (Khodabandeh, 2022). Before presenting numerical results regarding the performance of bias-bounded ILS, we first derive expressions for the conditional solution $\hat{\tilde{b}}(\tilde{z}_1)$ and its variance σ_0^2, addressing how they govern the function $P(\tilde{z}_1)$ in (12).

2. Canonical Differencing Transformation

To derive $\hat{\tilde{b}}(\tilde{z}_1)$, we first show the dependency of the float solutions $\hat{x}$ and $\hat{\tilde{z}}_1$ on the estimable bias $\tilde{b}$. This can be achieved by making use of the Canonical Differencing (CD) transformation (Khodabandeh and Teunissen, 2018). Accordingly, we transform the system of observation equations (8) into four *uncorrelated* parts. The CD transformation, denoted by the invertible matrix T, establishes the relation $y = T^{-1}(Ty)$ such that the variance matrix of the corresponding transformed observable vector Ty becomes *block-diagonal*. Let the joint variance matrix of the phase and code observation vectors ϕ and p be given by

$$\mathsf{D}\left(\begin{bmatrix} \phi \\ p \end{bmatrix}\right) = \begin{bmatrix} 2\,\sigma_\phi^2\, W^{-1} & 0 \\ 0 & 2\,\sigma_p^2\, W^{-1} \end{bmatrix} \tag{13}$$

The symbol $\mathsf{D}(\cdot)$ denotes the dispersion operator. The zenith-referenced standard deviations of the undifferenced (UD) phase and code data are denoted by σ_ϕ and σ_p, respectively. Note that both the phase and code data generally become less precise the smaller the satellite elevation becomes. Therefore, the $n \times n$ diagonal weight matrix W models the elevation-dependency of the data. The presence of the number 2 in (13) indicates that the variance of the SD measurements is twice that of their UD

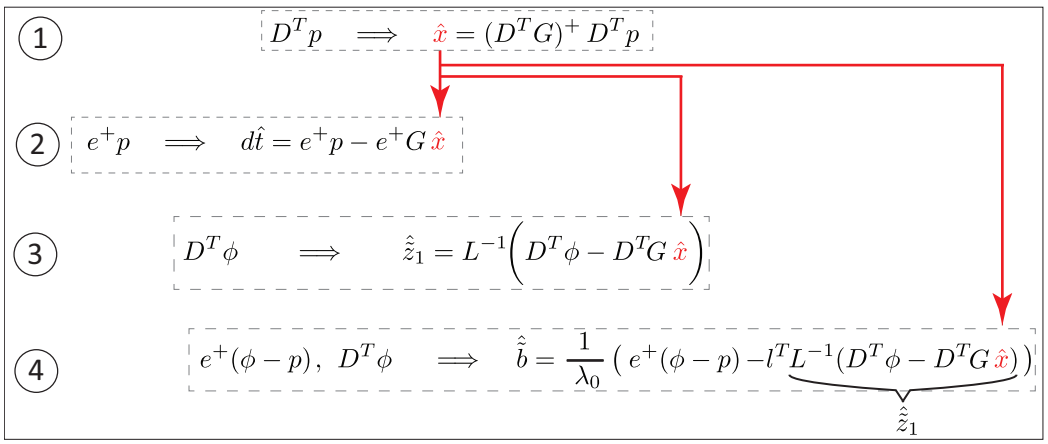

Figure 2: A diagram showing how the float solution of the position $\hat{x}$ propagates into the remaining float solutions of the short-baseline model (8), cf. the transformed model (14). The necessary and sufficient condition for the bias solution $\hat{\tilde{b}}$ to become 'uncorrelated' with $\hat{x}$ is that $l^T L^{-1} D^T G = 0$, that is, when $\hat{\tilde{b}}$ does not functionally depend on $\hat{x}$.

counterparts, assuming that the measurements of the two receivers are uncorrelated. Given the variance matrix, the sought-for transformation reads $T = [D, e^{+T}]^T$, where the $(n-1) \times n$ matrix D^T performs between-satellite differences, while the $1 \times n$ vector $e^+ = (1/e^T W e) e^T W$ performs weighted-averaging. Therefore, $D^T e = 0$ and $e^+ e = 1$. Since the vector ΛZ_2 is parallel to e (cf. 7), we also have the identities $D^T \Lambda Z_2 = 0$ and $e^+ \Lambda Z_2 = \lambda_0$. Post-multiplying each of the phase and code data ϕ and p, in (8), with the transformation matrix T, would then give the following four uncorrelated parts

$$\begin{aligned} &\textcircled{1}\ \mathsf{E}(D^T p) = [D^T G]\, x, && \textcircled{2}\ \mathsf{E}(e^+ p) = [e^+ G]\, x + dt \\ &\textcircled{3}\ \mathsf{E}(D^T \phi) = [D^T G]\, x + L \tilde{z}_1, && \textcircled{4}\ \mathsf{E}(e^+ \phi) = [e^+ G]\, x + dt + l^T \tilde{z}_1 + \lambda_0\, \tilde{b} \end{aligned} \tag{14}$$

with $L = D^T \Lambda Z_1$ and $l^T = e^+ \Lambda Z_1$. A closer look at (14) reveals that only model ① has redundancy, in which the number of DD observations $D^T p$ is more than the number of involved estimable parameters (i.e. x) when $n \geq 4$. The other three models have *no* redundancy. In model ②, the observation $e^+ p$ is reserved for the estimable clock parameter dt. In model ③, the DD observations $D^T \phi$ are reserved for the integer-estimable ambiguities $\tilde{z}_1$. And finally in model ④, the observation $e^+ \phi$ is reserved for the estimable bias $\tilde{b}$. As a result, least-squares estimation is only applied to ① so as to obtain the position's float solution as $\hat{x} = (D^T G)^+ D^T p$, with the least-squares matrix $(D^T G)^+ = (G^T D \bar{W} D^T G)^{-1} G^T D \bar{W}$, where $\bar{W} = (D^T W^{-1} D)^{-1}$. The remaining solutions follow then by the forward substitution of $\hat{x}$ into ②, ③ and ④.

A diagram showing how the position's float solution $\hat{x}$ propagates into the other solutions is presented in Figure 2. Since the transformed observations of the four models in (14) are mutually uncorrelated, checking the presence of correlation between the solutions has been made straightforward. For instance, the correlation between the clock solution $d\hat{t}$ and the position solution $\hat{x}$ is only felt through the 1×3 vector $e^+ G$. Therefore, $d\hat{t}$ and $\hat{x}$ would have been uncorrelated if $e^+ G = 0$, i.e., if the (weighted) average of the satellite line-of-sight unit vectors is zero. Since visible satellites are above the horizon (by definition), having positive values for the up-component of their corresponding unit vectors, the condition $e^+ G = 0$ never holds. Therefore, the position solution $\hat{x}$ is *always* correlated with the receiver clock solution $d\hat{t}$.

For the objective of this study, we are interested in knowing if the float solutions $\hat{x}$ and $\hat{\tilde{z}}_1$ are correlated with the bias solution $\hat{\tilde{b}}$ to verify the validity of the two propositions stated above on Page 2. According to Figure 2, the position solution $\hat{x}$ is not correlated with $\hat{\tilde{b}}$ when $l^T L^{-1} D^T G = 0$, that is, when $\hat{\tilde{b}}$ does not depend functionally on $\hat{x}$. To have $\hat{\tilde{b}}$ also uncorrelated with $\hat{\tilde{z}}_1$, the condition $l^T L^{-1} = 0$ (or equivalently $l = 0$) should hold. Therefore, with $l = 0$, both the position solution $\hat{x}$ and ambiguity solution $\hat{\tilde{z}}_1$ would have been uncorrelated with the bias solution $\hat{\tilde{b}}$. Under this condition, constraining the transformed phase bias b (like $b = 0$) to resolve the extra ambiguity $\tilde{z}_2$ does *not* pay off. However, equality $l = 0$ does indeed *never* occur (Appendix), meaning that at least the second proposition stated on Page 2 *always* remains valid for model (8), irrespective of the signal frequencies of the transmitters. However, the extent to which the bias constraint $|b| \leq h$ can be beneficial for ambiguity-resolved positioning depends on the model's strength (e.g., number of transmitters) and the structure of the involved signal frequencies.

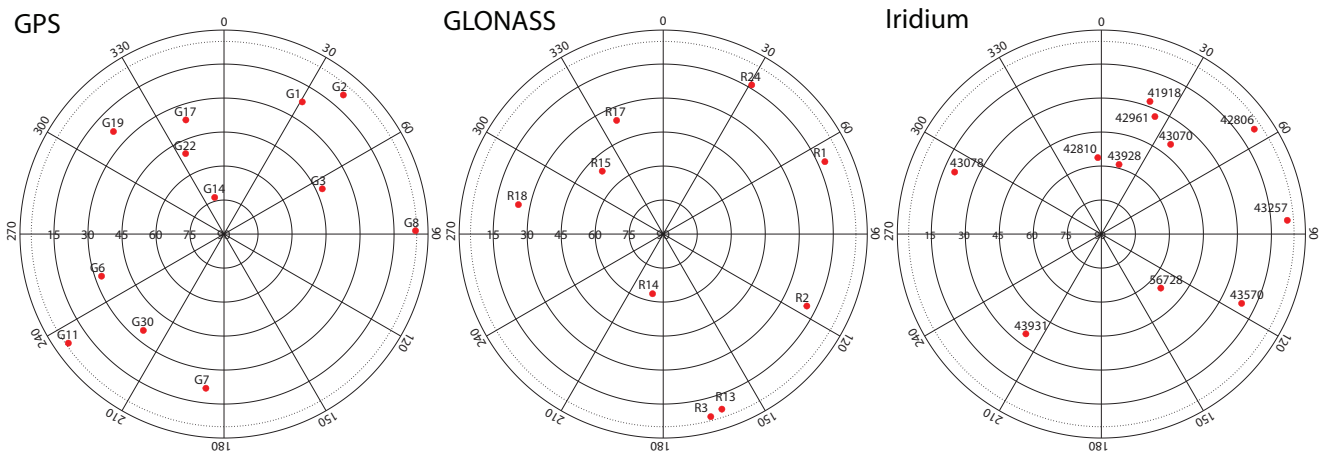

Figure 3: Skyplots of three satellite configurations as used in this study. The GPS and GLONASS configurations are with respect to IGS station ABMF (located in France), whereas the Iridium configuration is respect to IGS station ALRT (located in Canada), on 26 June 2024.

Before discussing how to incorporate $|b| \leq h$ into the model, we first highlight the role of the float ambiguity solution $\hat{\tilde{z}}_1$ in governing the correlation between the position solution $\hat{x}$ and the bias solution $\hat{\tilde{b}}$. As shown in Figure 2, the dependence of $\hat{\tilde{b}}$ on $\hat{x}$ is sensed only through the presence of $\hat{\tilde{z}}_1$. If the integer-estimable ambiguity vector $\tilde{z}_1$ is known, the bias solution $\hat{\tilde{b}}$ would be replaced by the *conditional* version

$$\hat{\tilde{b}}(\tilde{z}_1) = \frac{1}{\lambda_0}\{(e^+(\phi - p)) - l^T\tilde{z}_1\} \tag{15}$$

Since the conditional bias solution (15) is a function of the observations $e^+\phi$ and e^+p, it is *uncorrelated* with the position solution $\hat{x}$ (see Figure 2). An application of the variance propagation law to (15) gives the variance of $\hat{\tilde{b}}(\tilde{z}_1)$ as

$$\sigma_0^2 = \frac{2}{\lambda_0^2}\frac{\sigma_\phi^2 + \sigma_p^2}{e^T W e} \tag{16}$$

Despite being uncorrelated with $\hat{x}$, the conditional bias solution $\hat{\tilde{b}}(\tilde{z}_1)$ and its variance σ_0^2 can play a decisive role in *penalizing* possible outcomes of the IAR process, allowing for higher success rates of resolving $\tilde{z}_1$. According to (12), the role of function $P(\tilde{z}_1)$ becomes more pronounced if the variance σ_0^2 is considered small *relative* to the ambiguity variance matrix $Q_{\hat{\tilde{z}}_1\hat{\tilde{z}}_1}$. As σ_0 is inversely proportional to the base wavelength λ_0 (see 16), the bias constraint $|b| \leq h$ can therefore be more decisive through the function $P(\tilde{z}_1)$, the larger the wavelength λ_0 becomes. In the GPS case, we have $\lambda_0 \approx 19$ [cm] for the L1-frequency. In the GLONASS FDMA case however, the base wavelength takes a much larger value of $\lambda_0 \approx 533$ [m], leading to a much more precise conditional bias solution $\hat{\tilde{b}}(\tilde{z}_1)$. The GLONASS IAR performance is therefore expected to benefit more from the constraint $|b| \leq h$ than that of its GPS counterpart.

IV. BIAS-BOUNDED ILS AT WORK

To gain initial insight into the role of the constraint $|b| \leq h$, we first consider an extreme case in which the phase bias b is assumed to be zero, that is, $\tilde{b} = \tilde{z}_2$. Under this assumption, the estimable ambiguity vector a, in (8), is integer, i.e. $a = Z_1\,\tilde{z}_1 + Z_2\,\tilde{z}_2 = z$. To verify whether or not resolving the extra ambiguity $\tilde{z}_2$ can improve the IAR performance, one would therefore need to compare the following two ambiguity-fixing strategies

$$\begin{aligned} &1 \text{ - Full IAR :} \quad a = Z_1\,\tilde{z}_1 + Z_2\,\tilde{z}_2, \qquad (\tilde{z}_1 \in \mathbb{Z}^{(n-1)},\ \tilde{z}_2 \in \mathbb{Z}) \\ &2 \text{ - Partial IAR :} \quad a = Z_1\,\tilde{z}_1 + Z_2\,\tilde{z}_2, \qquad (\tilde{z}_1 \in \mathbb{Z}^{(n-1)},\ \tilde{z}_2 \in \mathbb{R}) \end{aligned} \tag{17}$$

Resolving the full set of ambiguities $[\tilde{z}_1^T, \tilde{z}_2]^T$ may lead to a *lower* ambiguity success-rate, particularly when the float solutions of $\tilde{z}_1$ and $\tilde{z}_2$ are weakly correlated. This means that imposing the bias constraint $b = 0$ may *not* always enhance ambiguity-resolved positioning performance and could, in some cases, degrade it. To see if switching to full IAR is preferred over its partial IAR version in (17), let us compare their performances in terms of Ambiguity Dilution Of Precision (ADOP). ADOP measures the

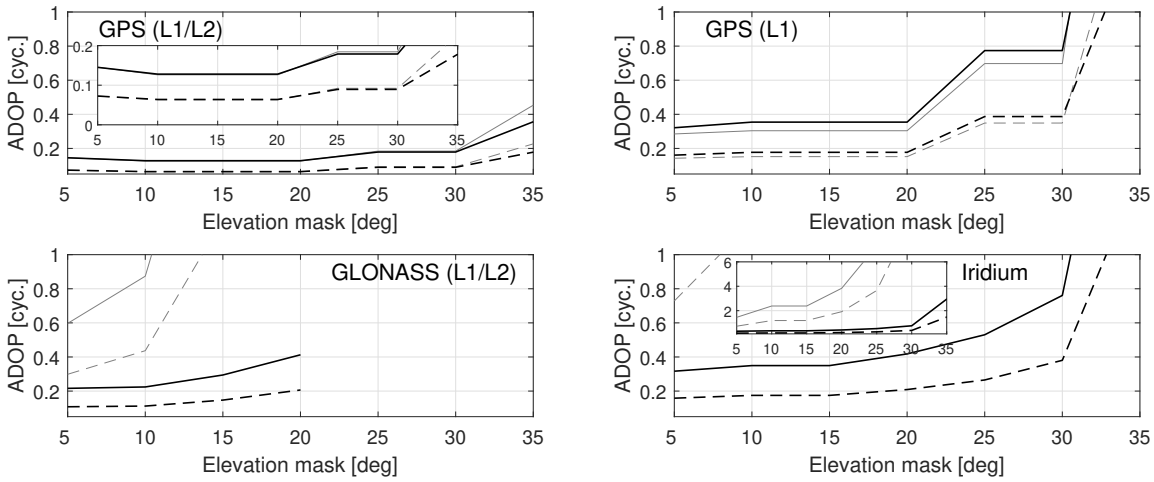

Figure 4: ADOP values as function of the satellite elevation mask, corresponding to the three satellite configurations in Figure 3. The black lines correspond to the SD case of $z = Z_1\tilde{z}_1 + Z_2\tilde{z}_2$, and the gray lines correspond to the integer-estimable case of $\tilde{z}_1$. The solid and dashed lines indicate single- and quadruple-epoch cases, respectively. The zenith-referenced code and phase measurement standard deviations (undifferenced) are, respectively, set to $\sigma_p = 0.3$ [m] and $\sigma_\phi = 0.003$ [m]. The sine-squared function of the satellite elevation is used to form the diagonal entries of the weight matrix W in (13).

average precision of the float ambiguity solution (Teunissen, 1997). From the ADOP, one can roughly infer the bootstrapped ambiguity success-rate. The smaller the ADOP, the higher the the stated success-rate becomes. As a rule of thumb, when the ADOP is smaller than 0.14 cycles, the stated success-rate is larger than 99% (Odijk and Teunissen, 2008). We compare such ADOP values for three different satellite configurations (Figure 3). The results are presented in Figure 4. The ADOP values are shown as a function of the satellite elevation mask. As the elevation mask increases from 5 to 35 degrees, the number of tracked satellites decreases, leading to a weaker model in the sense of having fewer redundant measurements. Consequently, ADOP increases the higher the elevation mask. As the number of tracked GLONASS satellites becomes less than the minimum required value of $n = 4$, no ADOP values are shown when the elevation mask is larger than 20 [degrees]. As shown in Figure 4, apart from the GPS single-frequency case (L1), the ADOP values of the SD case (black lines) are *smaller* than their versions obtained for the integer-estimable case (gray lines). This shows that imposing the bias constraint $b = 0$ can improve the IAR performance. However, the size of the stated improvement differs notably across different satellite systems. While the GLONASS and Iridium ADOPs can experience a considerable reduction in their values, the GPS dual-frequency case (L1/L2) slightly decreases. As stated previously, this is due to the much larger base wavelengths of the GLONASS and Iridium signal frequencies (see 16 and 12). The figure also compares single-epoch ADOP values (solid lines) with their quadruple-epoch versions (dashed lines), where a measurement sampling-rate of 1 second is considered. As indicated, ADOP decreases as more redundant measurements are collected at multiple epochs.

To better understand the bias-bounded ambiguity-resolved positioning performance, we simulate normally-distributed measurements for the Iridium satellite configuration in Figure 3. Four simulated cases are considered: 1) the phase bias is known to be zero over two epochs, 2) the phase bias is known to be zero over four epochs, 3) the phase bias b is constant over two epochs with constraint $|b| \leq 0.02$, and 4) the phase bias b is constant over four epochs with constraint $|b| \leq 0.02$. For each simulated case, 10,000 normally-distributed simulated samples are generated. For the nonzero bias cases, the time-constant bias b is different in each simulation and varies from -0.02 to 0.02 [cycles]. The corresponding positioning results are shown in Figure 5. The figure compares the float positioning solutions (blue dots) with their $\tilde{z}_1$-fixed (gray dots), and bias-bounded ILS versions (black dots). In terms of root-mean-squared-errors (RMSE), the performance of the bias-bounded ILS solutions (black dots) is shown to be better than that of the $\tilde{z}_1$-fixed solutions (gray dots). While these solutions are more accurate than their float counterparts, the bias-bounded ILS solutions, particularly for the up-component, outperform the $\tilde{z}_1$-fixed solutions in terms of accuracy. It is also important to note that the decrease in the RMSE of the float solutions does not follow the 1-over-$\sqrt{k}$ rule (k: number of epochs), as one often observes for high-rate GNSS cases (Teunissen, 1997). This is due to the rapid change in the receiver-to-LEO satellite line-of-sight unit vectors on which both the G- and W-matrices are based, see (4) and (13).

Next to the rather small bias value of 0.02 [cycles], we also examine the effect of different bias values in Figure 6. The figure shows the empirical Cumulative Distribution Function (CDF) of the position error-magnitude corresponding to the GLONASS (left) and Iridium (right) satellite configurations. As the bound h increases, the constraint is loosened, the bias-bounded ILS solutions (gray curves) tend to behave more similar to their $\tilde{z}_1$-fixed versions. For the extreme case of $h = 0.5$ [cycles], the

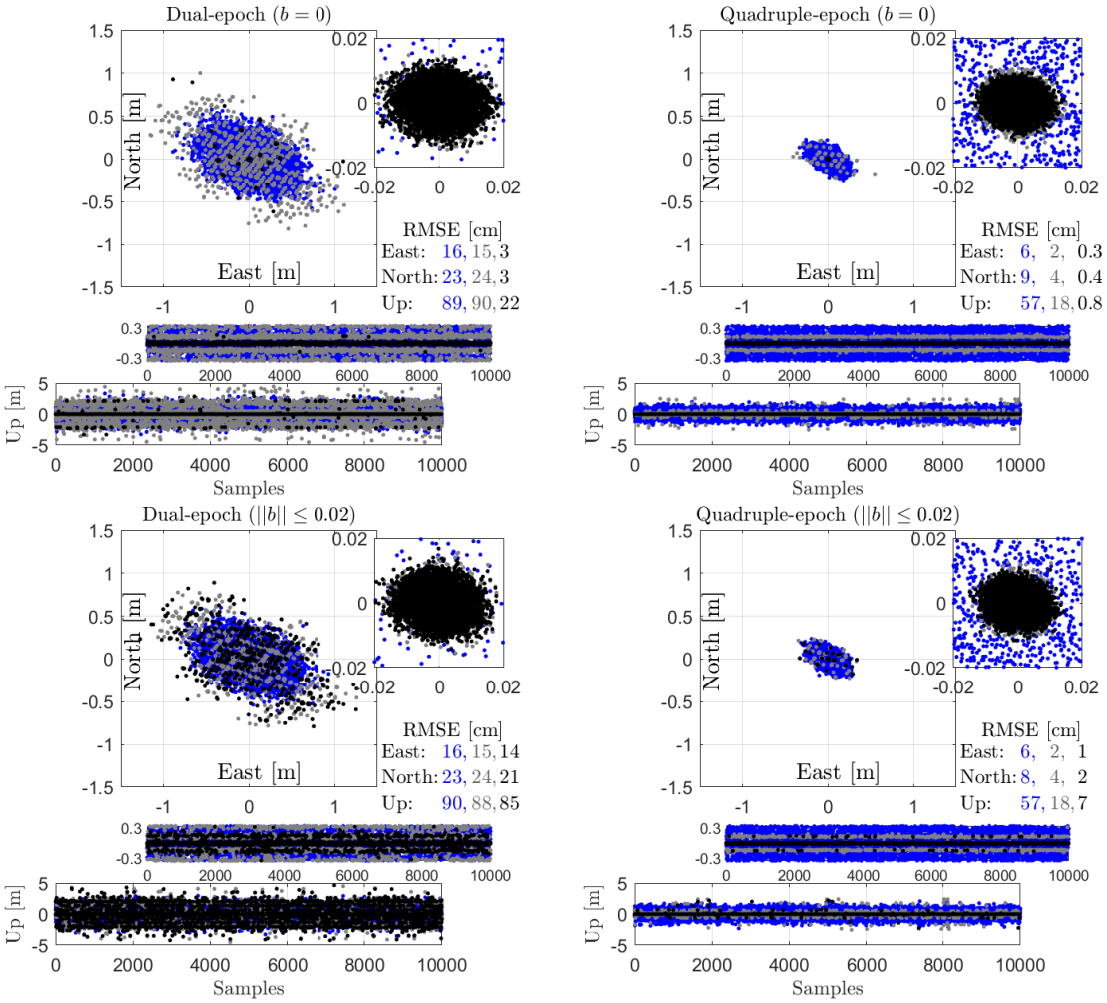

Figure 5: Short-baseline positioning errors (East-North scatters and Up-time series) corresponding to the Iridium satellite configuration in Figure 3. The blue, gray and black dots correspond to float, $\tilde{z}_1$-fixed, and bias-bounded ILS solutions, respectively. Four simulated cases are considered: 1) the phase bias is known to be zero over two epochs (top-left), 2) the phase bias is known to be zero over four epochs (top-right), 3) the phase bias b is constant over two epochs with constraint $|b| \leq 0.02$ (bottom-left), and 4) the phase bias b is constant over four epochs with constraint $|b| \leq 0.02$ (bottom-right). For each simulated case, 10,000 normally-distributed simulated samples are generated. For the nonzero bias cases, the time-constant bias b is different in each simulation and varies from -0.02 to 0.02 [cycles]. The RMSE values [cm] of each case are distinguished by their corresponding colors.

results get identical to the $\tilde{z}_1$-fixed solutions (Khodabandeh and Teunissen, 2024). Compared to their float versions (blue curves), the bias-bounded ILS solutions exhibit a smaller position error-magnitude when the bound h is way smaller than 0.5 [cycles]. For instance, for the GLONASS case, only 40% of the float results have a sub-meter position error-magnitude, while only 30% of the corresponding $\tilde{z}_1$-fixed solutions have such an error-magnitude. By imposing the constraint $|b| \leq 0.05$ cycles, more than 57% of the bias-bounded ILS solutions have a sub-meter error-magnitude. In the case of Iridium, over 90% of the bias-bounded ILS solutions have an error-magnitude smaller than 20 [cm] using the same bias constraint. However, it is important to remark that such outcomes are expected when the phase bias b is bounded and smaller than h. When the bias constraint $|b| \leq h$ is misspecified, bias-bounded ILS may give less accurate solutions than those of the $\tilde{z}_1$-fixed case (Khodabandeh and Teunissen, 2024).

V. CONCLUDING REMARKS

In this contribution we investigated the role of non-integer phase biases in influencing the model's IAR performance, showing how the bias constraint $||b|| \leq h$ can improve the ambiguity-resolved positioning performance. After reviewing the integer-estimable parametrized model for short-baslines (8), we first addressed the interrelationship between the involved float solutions,

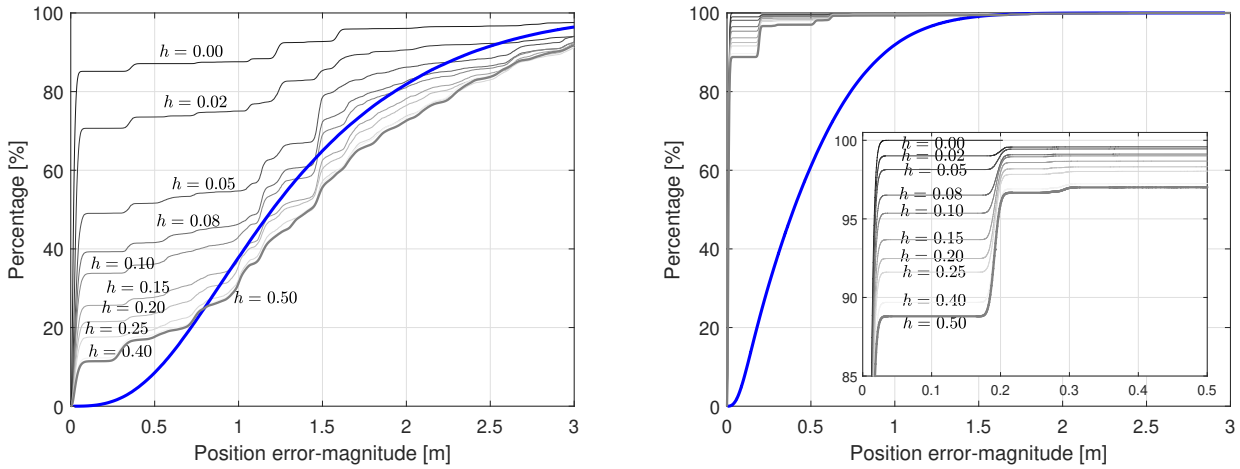

Figure 6: Empirical CDF of the position error-magnitude (quadruple-epoch case) corresponding to the GLONASS, L1-only (left) and Iridium (right) satellite configurations for different bias bounds h [cycles], cf. Figure 3. The blue and gray curves correspond to float and bias-bounded ILS solutions, respectively. For each of the bias constraints $|b| \leq h$, 10,000 normally-distributed samples are simulated. The time-constant bias b is different in each simulation and varies from $-h$ to $+h$ [cycles].

i.e. the solutions for which the integerness of the phase ambiguities z in $\tilde{a} = z + Re\,\tilde{b}$ is discarded (Figure 2). It is shown how the float position solution propagates into the remaining solutions, making them correlated. Importantly, the nonzero correlation between the bias solution $\hat{\tilde{b}}$ and the position $\hat{x}$ and ambiguity solution $\hat{\tilde{z}}_1$ indicates that information about $\tilde{b} = b + \tilde{z}_2$ can potentially improve the precision of both $\hat{x}$ and $\hat{\tilde{z}}_1$. Precision improvement in the float ambiguities $\hat{\tilde{z}}_1$ leads to a higher ambiguity success-rate, thereby enhancing the the performance of corresponding ambiguity-resolved positioning.

Would the boundedness property of the GLONASS FDMA phase-biases (Figure 1) carry over to other frequency-varying carrier-phase signals like those of LEO satellites, it is then worthwhile to quantify the extent to which imposing the constraint $|b| \leq h$ can bring position precision improvement. We therefore employed the bias-bounded ILS estimation (cf. 9) and showed how the function $P(\tilde{z}_1)$ is aimed to penalize possible outcomes of the IAR process. With the aid of simulated results, it was illustrated that one can leverage both the bias constraint $|b| \leq h$ and the number of epochs to obtain positioning results that are considerably more accurate than their both float and $\tilde{z}_1$-fixed counterparts.

VI. APPENDIX

We prove why the $1 \times (n-1)$ vector $l^T = e^+ \Lambda Z_1$ cannot be a zero vector. We confine our proof to the case $W = I_n$. Let us assume that $l = 0$. Thus $e^+ \Lambda Z_1 = 0$. Substitution of $e^+ = (1/n)e^T$, together with $\Lambda = \lambda_0\, R^{-1}$, gives $e^T R^{-1} Z_1 = 0$. Therefore, the column-space of the integer matrix Z_1 must be orthogonal to the vector $R^{-1}e$. As a result, this matrix can be expressed as $Z_1 = RDX$ for some *integer* matrix $X \in \mathbb{Z}^{(n-1)\times(n-1)}$. As an admissible integer transformation, matrix $[Z_1, Z_2]$ (where $Z_2 = Re$) has a determinant equal to ± 1 (Teunissen, 1995), that is, $\det([RDX, Re]) = \pm 1$. Post-multiplying $[Z_1, Z_2]$ with $[D, u_1]^T R^{-1}$ and taking the determinant of the product give

$$\pm \frac{1}{\det(R)} = \det\left(\begin{bmatrix} D^T DX & 0 \\ u_1^T DX & 1 \end{bmatrix} \right) = \det(D^T D)\det(X) \tag{18}$$

where $u_1 = [1, 0, \ldots, 0]^T \in \mathbb{Z}^n$. The first equality in (18) follows as matrix $[D, u_1]^T$ is itself an admissible integer transformation, i.e., $\det([D, u_1]) = \pm 1$ (Khodabandeh and Teunissen, 2019). The second equality follows because the determinant of a lower block-triangular matrix is the product of the determinants of its diagonal sub-matrices. Using the identity $\det(D^T D) = n$, we obtain from (18) that $\det(X) = \pm \frac{1}{n \det(R)} \notin \mathbb{Z}$. This contradicts the integerness of matrix X.

ACKNOWLEDGEMENTS

This research was partially supported by the Australian Research Council's Industrial Transformation Research Programme [IH210100048].

REFERENCES

Aggrey, J. and Bisnath, S. (2016). Dependence of GLONASS Pseudorange Inter-frequency Bias on Receiver–Antenna Combination and Impact on Precise Point Positioning. *NAVIGATION*, 63(4):379–391.

Banville, S., Collins, P., and Lahaye, F. (2018). Model comparison for GLONASS RTK with low-cost receivers. *GPS Solutions*, 22(2):1–12.

Brack, A., Männel, B., and Schuh, H. (2021). GLONASS FDMA data for RTK positioning: a five-system analysis. *GPS solutions*, 25(1):1–13.

Henkel, P., Mittmann, U., and Iafrancesco, M. (2016). Real-time kinematic positioning with GPS and GLONASS. In *2016 24th European Signal Processing Conference (EUSIPCO)*, pages 1063–1067. IEEE.

Hofmann-Wellenhof, B., Lichtenegger, H., and Wasle, E. (2008). *GNSS: Global Navigation Satellite Systems: GPS, GLONASS, Galileo, and More*. Springer, New York.

Kassas, Z., Morales, J., and Khalife, J. (2019). New-age satellite-based navigation–STAN: simultaneous tracking and navigation with LEO satellite signals. *Inside GNSS Magazine*, 14(4):56–65.

Khalife, J. and Kassas, Z. Z. M. (2023). Performance-driven design of carrier phase differential navigation frameworks with megaconstellation LEO satellites. *IEEE Transactions on Aerospace and Electronic Systems*, 59(3):2947–2966.

Khodabandeh, A. (2022). Bias-bounded Estimation of AmbiguiTy: a method for radio interferometric positioning. *IEEE Transactions on Signal Processing*, 70:3042–3057.

Khodabandeh, A. and Teunissen, P. J. G. (2018). On the impact of GNSS ambiguity resolution: geometry, ionosphere, time and biases. *J Geod*, 92(6):637–658.

Khodabandeh, A. and Teunissen, P. J. G. (2019). Integer estimability in GNSS networks. *J Geod*, 93(9):1805–1819.

Khodabandeh, A. and Teunissen, P. J. G. (2023). Ambiguity-fixing in frequency-varying carrier phase measurements: Global Navigation Satellite System and Terrestrial examples. *NAVIGATION*, 70(2).

Khodabandeh, A. and Teunissen, P. J. G. (2024). Bias-constrained integer least squares estimation: distributional properties and applications in GNSS ambiguity resolution. *Journal of Geodesy*, 98(5):40.

Maróti, M., Völgyesi, P., Dóra, S., Kusỳ, B., Nádas, A., Lédeczi, A., Balogh, G., and Molnár, K. (2005). Radio Interferometric Geolocation. In *Proceedings of the 3rd international conference on Embedded networked sensor systems*, pages 1–12.

Odijk, D. and Teunissen, P. J. G. (2008). ADOP in closed form for a hierarchy of multi-frequency single-baseline GNSS models. *J Geod*, 82(8):473–492.

Pratt, S. R., Raines, R. A., Fossa, C. E., and Temple, M. A. (1999). An operational and performance overview of the IRIDIUM low earth orbit satellite system. *IEEE Communications Surveys*, 2(2):2–10.

Shamaei, K. and Kassas, Z. M. (2019). Sub-meter accurate UAV navigation and cycle slip detection with LTE carrier phase measurements. In *Proceedings of the 32nd International Technical Meeting of the Satellite Division of The Institute of Navigation (ION GNSS+ 2019)*, pages 2469–2479.

Sleewaegen, J., Simsky, A., De Wilde, W., Boon, F., and Willems, T. (2012). Origin and compensation of GLONASS inter-frequency carrier phase biases in GNSS receivers. In *Proceedings of the 25th International Technical Meeting of the Satellite Division of The Institute of Navigation (ION GNSS 2012)*, pages 2995–3001.

Teunissen, P. J. G. (1993). Least-Squares Estimation of the Integer GPS ambiguities. In *Invited Lecture, Section IV Theory and Methodology, IAG General Meeting*, Beijing, China, August.

Teunissen, P. J. G. (1995). The invertible GPS ambiguity transformations. *Manuscripta Geodaetia*, 20:489–497.

Teunissen, P. J. G. (1997). A canonical theory for short GPS baselines. Part I: The baseline precision. *J Geod*, 71(6):320–336.

Teunissen, P. J. G. (1999). An optimality property of the integer least-squares estimator. *J Geod*, 73(11):587–593.

Teunissen, P. J. G. (2019). A new GLONASS FDMA model. *GPS Solut.*, 23:100.

Teunissen, P. J. G., de Jonge, P. J., and Tiberius, C. C. J. M. (1997). Performance of the LAMBDA method for fast GPS ambiguity resolution. *NAVIGATION*, 44(3):373–383.

Teunissen, P. J. G. and Khodabandeh, A. (2019). GLONASS ambiguity resolution. *GPS Solut.*, 23:101.

Teunissen, P. J. G. and Khodabandeh, A. (2022). PPP-RTK theory for varying transmitter frequencies with satellite and terrestrial positioning applications. *Journal of Geodesy*, 96(11):84.

Teunissen, P. J. G. and Montenbruck, O., editors (2017). *Springer Handbook of Global Navigation Satellite Systems*. Springer.

Teunissen, P. J. G. and Odijk, D. (2003). Rank-defect integer estimation and phase-only modernized GPS ambiguity resolution. *Journal of Geodesy*, 76(9):523–535.

Wang, Y., Ma, X., Chen, C., and Guan, X. (2015). Designing Dual-Tone Radio Interferometric Positioning Systems. *IEEE Trans. Signal Process.*, 63(6):1351–1365.

Wanninger, L. and Wallstab-Freitag, S. (2007). Combined processing of GPS, GLONASS, and SBAS code phase and carrier phase measurements. In *Proceedings of the 20th International Technical Meeting of the Satellite Division of The Institute of Navigation (ION GNSS 2007)*, pages 866–875.

Zaminpardaz, S., Teunissen, P. J. G., and Khodabandeh, A. (2021). GLONASS only FDMA + CDMA RTK: Performance and outlook. *GPS Solutions*, 25(96).